

SUPPLEMENTARY INFORMATION

Dynamins maintain nuclear envelope homeostasis and genome stability

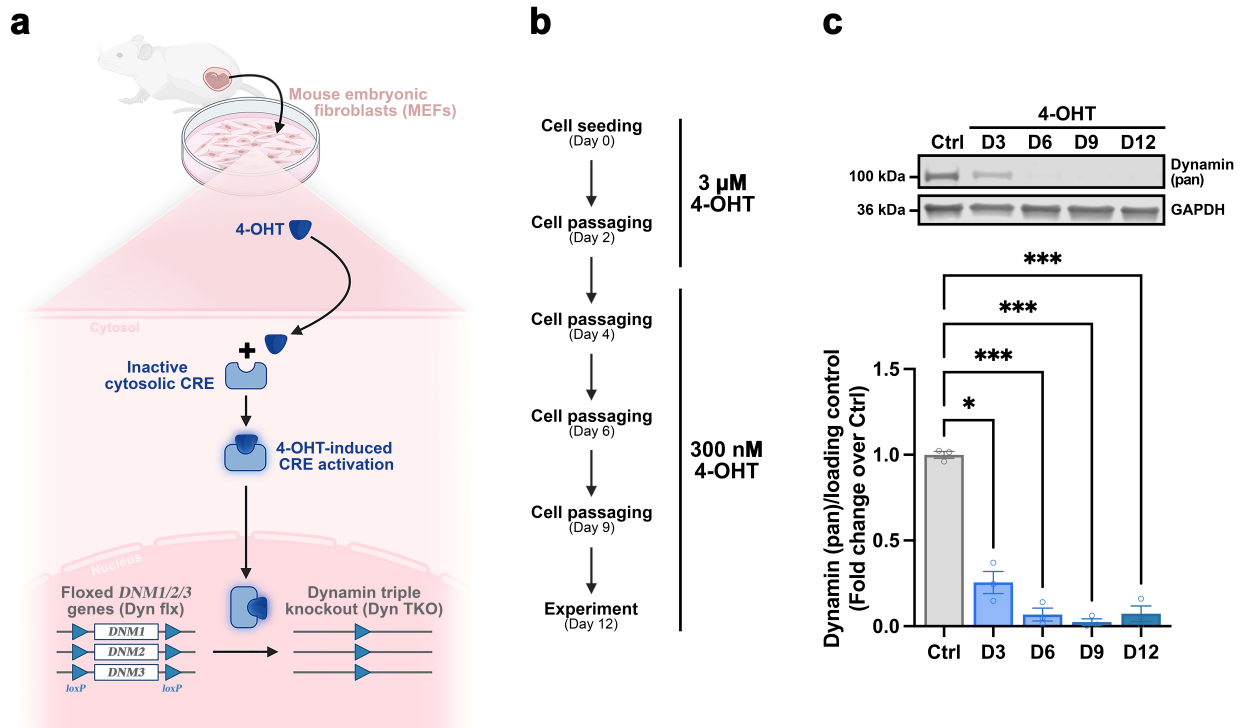
Célia Avelaira¹, Thibaud Martial², Loïc Carrique³, Rita Gaspar¹, Ana Caulino-Rocha¹, Izaak Myatt², Franz Wendler², Pauline Lascaux⁴, Misha Le Claire³, James Bancroft², Carl Smythe⁵, Kristijan Ramadan^{4,6}, Nuno Raimundo^{1,7,8}, Ira Milosevic^{1,2 §}

§ Corresponding author: Ira.Milosevic@well.ox.ac.uk

In this document:

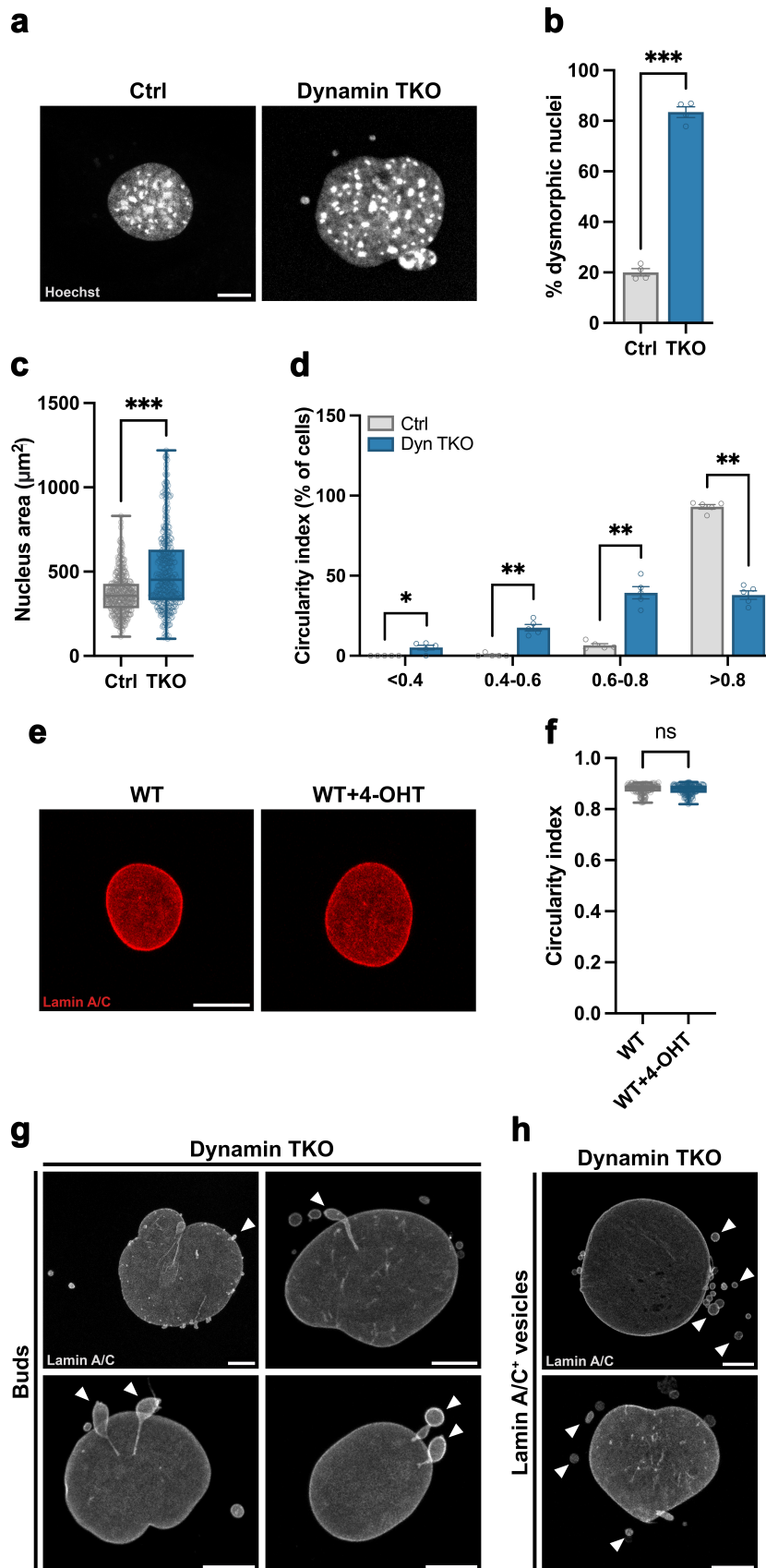
- **SUPPLEMENTARY FIGURES**
- **SUPPLEMENTARY TABLE 1**
- **SUPPLEMENTARY METHODS**

SUPPLEMENTARY FIGURES



Supplementary Figure 1: Generation of dynamin TKO cells.

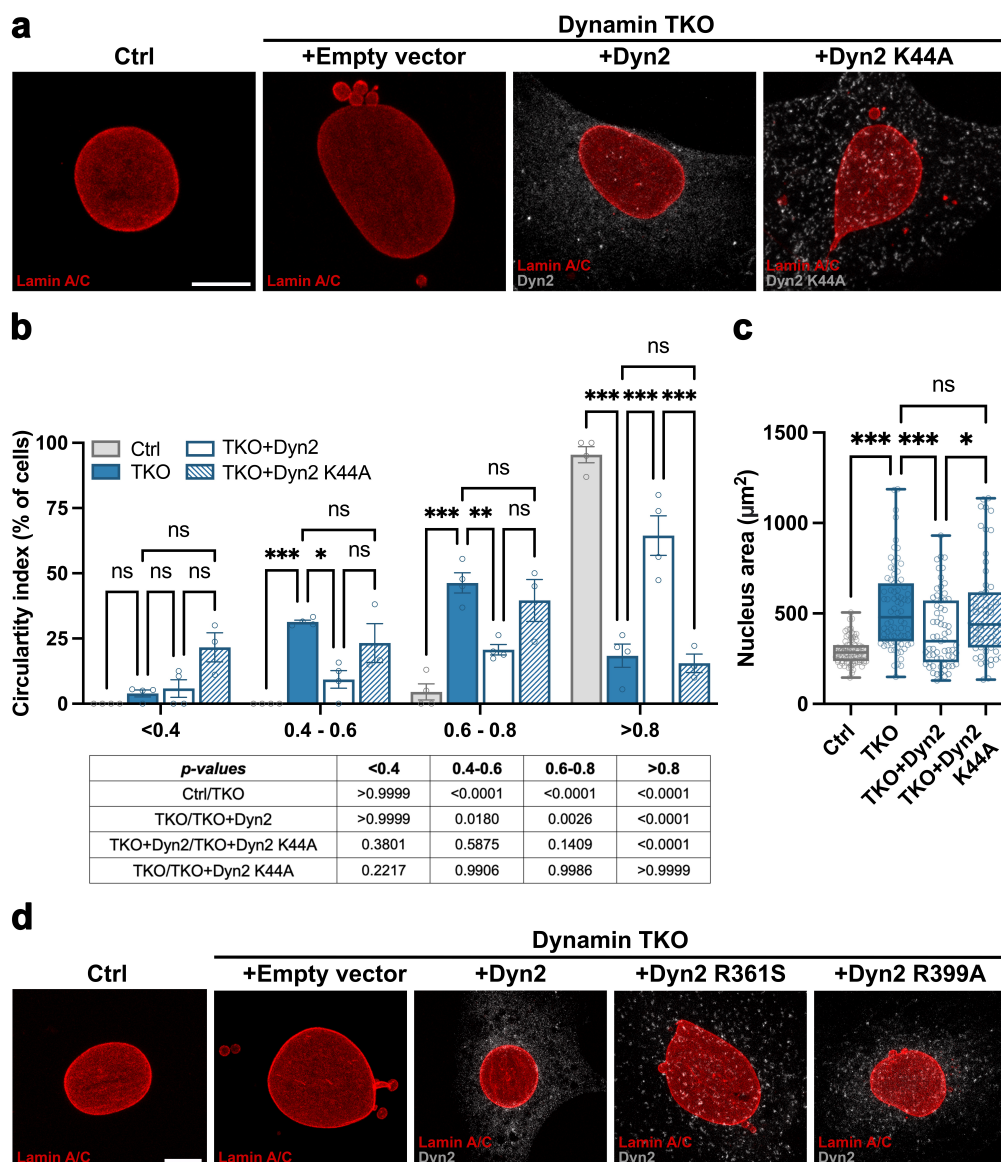
(a-b) Schematic representation of the experimental approach used, including the LoxP/LoxP recombination system (a) and of the methodology applied to generate dynamin TKO cells (b). Created in BioRender. Raimundo, N. (2026) <https://BioRender.com/ygmujci>. **(c)** Western blot (top) and respective quantification (bottom) of dynamin 1,2,3 expression levels in control (EtOH-treated) and 4-hydroxytamoxifen (4-OHT)-treated cells after 3, 6, 9 and 12 days of treatments. Note that dynamin expression is nearly abolished 6 days post-4-OTH treatment, and dynamin TKO cells are used for experiments after that time point. Three biological replicates/condition. Data are presented as bar charts with mean \pm SEM, *p<0.05; ***p<0.001. Statistical analyses were performed using one-way ANOVA followed by post-hoc Dunnett's multiple comparisons test (p=0.0200, p=0.0006, p<0.0001, p=0.0010). 4-OHT, 4-hydroxytamoxifen; Ctrl, Control; TKO, Triple knockout.



Supplementary Figure 2: Altered morphology and increased nuclear size in dynamin TKO cells.

(a-b) Representative images of DAPI stained control and dynamin-TKO cells (a), and respective quantification of dysmorphic nuclei (b). Scale bar 10 μ m. Four independent

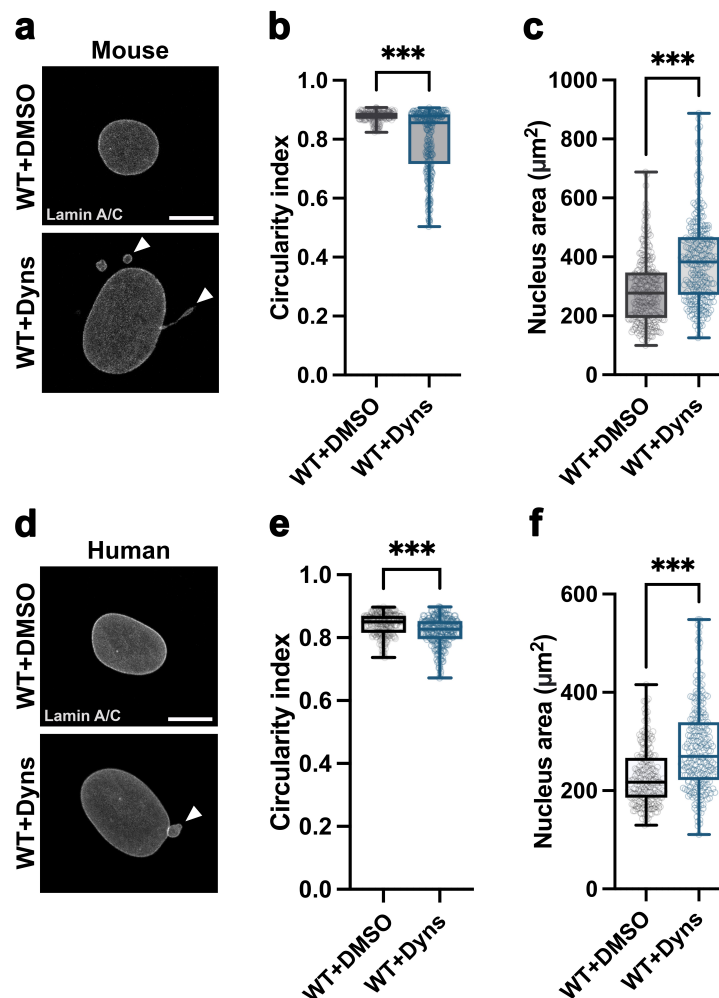
biological replicates; >500 cells/condition. These experiments were also done with Hoechst and SPY555-DNA probes, with indistinguishable results. **(c)** Quantification of nuclear area in control and dynamin-TKO cells. Four independent biological replicates; >370 cells/condition. **(d)** Distribution of circularity index among control and dynamin TKO cells. Binned data from Figure 1c. Five independent biological replicates; >317 cells/condition. **(e-f)** Representative images of lamin-A/C immunostained nuclei in wild-type (WT; DMSO treated) and 4-OHT treated WT mouse fibroblasts; no accumulation of nuclear dysmorphisms was observed in cells treated with 4-OHT (same concentration/duration as in dynamin-TKO cells) (e). Scale bar: 10 μ m. Quantification of circularity in WT (DMSO treated) and 4-OHT treated WT cells (f). Three independent biological replicates; >173 cells/condition. **(g)** Representative examples of lamin A/C immunostained nuclei with NE buds of different sizes (arrowheads) in dynamin TKO cells. Majority of dynamin TKO nuclei show small-sized buds (top left image), yet very large buds with long narrow necks are also seen. Lamin A/C-positive vesicles are occasionally seen in the proximity of large NE buds (top right). Some unusually large structures with very long narrow neck were also observed (bottom row). Scale bar 10 μ m. Four independent biological replicates. **(h)** Representative examples of accumulation of lamin A/C-positive vesicles in dynamin TKO cells immunostained against lamin A/C. Scale bar 10 μ m. Four independent biological replicates. Data are presented as bar charts with mean \pm SEM, and as box plots showing the 25th percentile (Q1), median, 75th percentile (Q3), and whiskers extending to the minimum and maximum values. Statistical significance is indicated as ns, not significant, * $p < 0.05$; ** $p < 0.01$; *** $p < 0.001$. Statistical analyses were performed using two-tailed unpaired Student's t-test with Welch's correction (b: $p < 0.0001$), two-tailed Mann-Whitney U-test (c: $p < 0.0001$, d: $p = 0.0476$, $p = 0.0079$, $p = 0.0079$, $p = 0.0079$, f: $p = 0.4656$). Ctrl, Control; TKO, Triple knockout.



Supplementary Figure 3: Transient expression of dynamin2-WT, but not of dynamin2-K44A rescues nuclear dysmorphisms in dynamin TKO cells.

(a) Representative images of lamin A/C immunostained nuclei in control and dynamin TKO cells after transfection with the pEGFP vector as control, dynamin2-WT or dynamin2-K44A mutant. Scale bar 10 μm. Four independent experiments. **(b)** Distribution of circularity index among control and dynamin TKO cells transfected with dynamin2-WT or dynamin2-K44A. Binned data from Figure 1h. Four (TKO, TKO+Dyn2) and three (TKO+Dyn2 K44A) independent biological replicates; >55 cells/condition. **(c)** Quantification of nuclear area, in control and dynamin TKO cells transfected with dynamin2-WT and dynamin2-K44A mutant. Four independent experiments; >56 cells/condition. **(d)** Representative images of lamin A/C immunostained nuclei in control, dynamin-TKO, TKO expressing dynamin-2, TKO expressing dynamin2-R361S and TKO expressing dynamin2-R399A for 24h. Scale bar 10 μm. Data are presented as bar charts with mean ± SEM, and as box plots showing the 25th percentile (Q1),

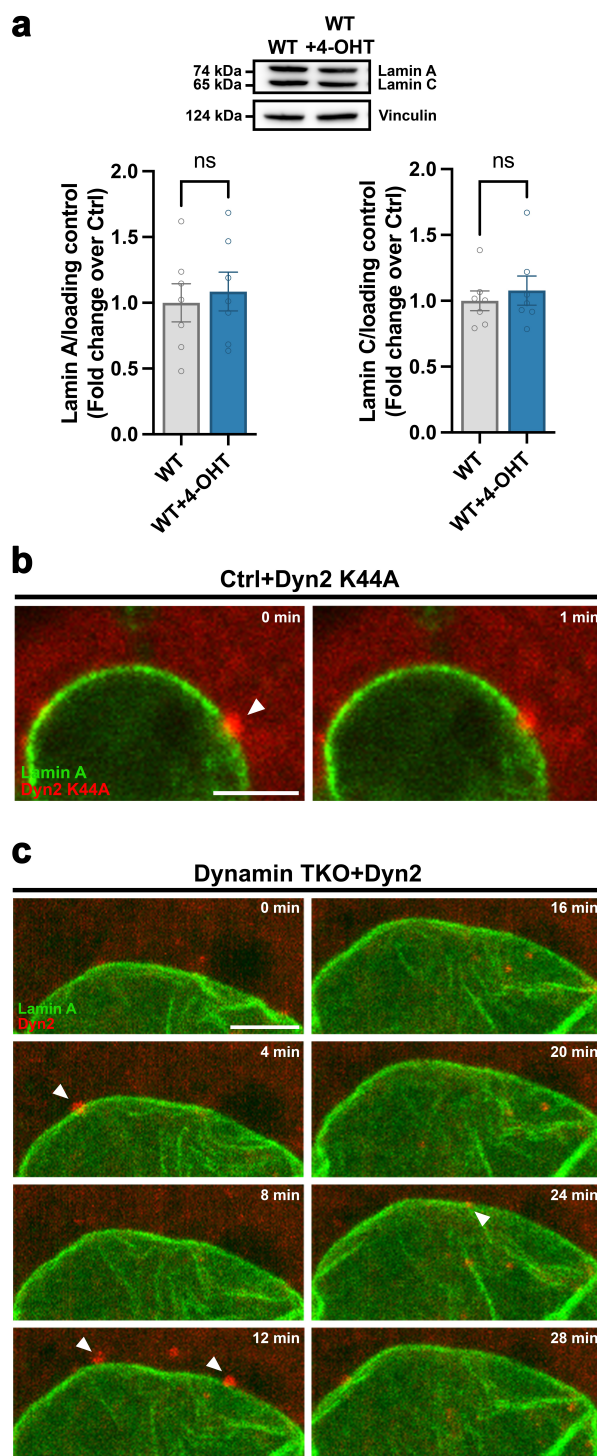
median, 75th percentile (Q3), and whiskers extending to the minimum and maximum values. ns, not significant; * $p < 0.05$; ** $p < 0.01$; *** $p < 0.001$. Statistical analyses were performed using two-way ANOVA followed by post-hoc Tukey's multiple comparisons test (b p -values are presented underneath the plot), one-way ANOVA Kruskal-Wallis test followed by post-hoc Dunn's multiple comparisons test (c: $p < 0.0001$, $p = 0.0007$, $p = 0.0420$, $p > 0.9999$). Ctrl, Control; TKO, Triple knockout.



Supplementary Figure 4: Nuclear dysmorphisms are also observed in wild-type mouse and human fibroblasts treated with the non-selective dynamin inhibitor dynasore.

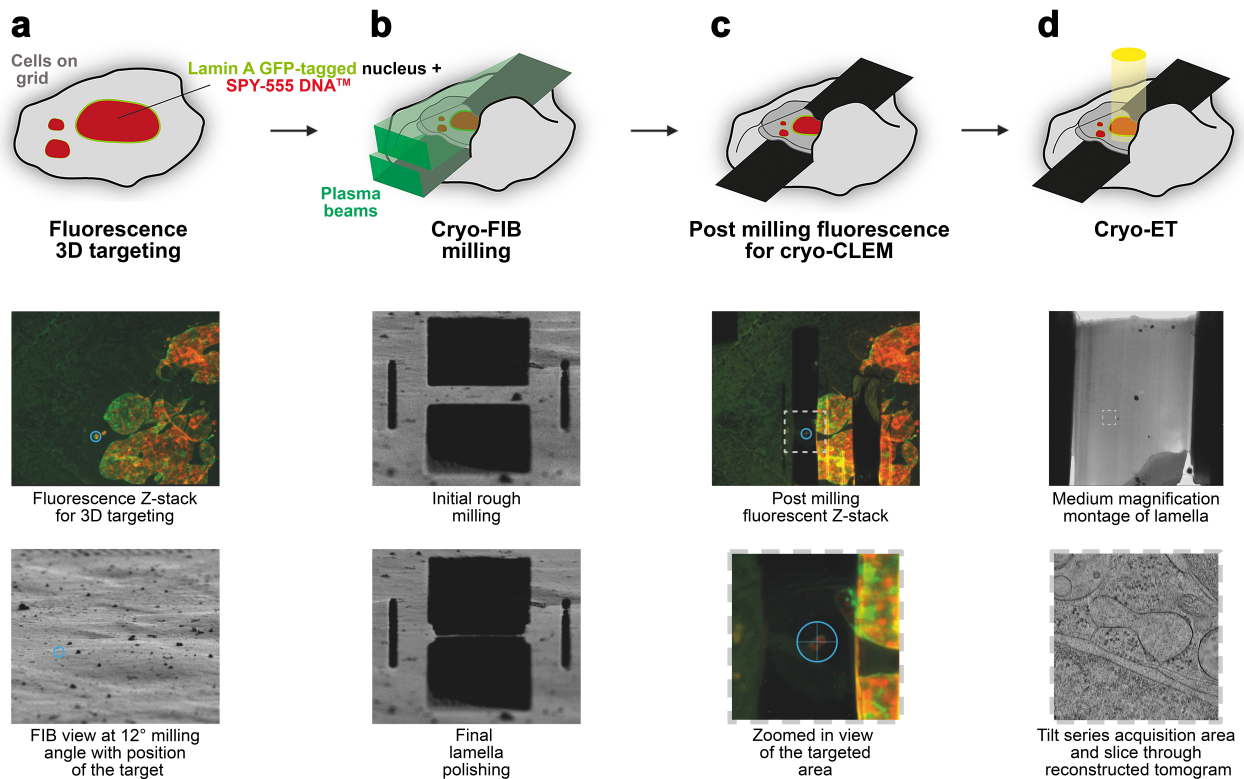
(a-c) Representative images of lamin A/C immunostained nuclei in wild-type mouse fibroblasts treated with DMSO (control) or dynasore (a), and respective quantification of nuclear circularity (b), and nucleus area (c). Scale bar 10 μm . Three independent biological replicates; >263 cells/condition. **(d-f)** Representative images of lamin A/C immunostained nuclei in wild-type human fibroblasts treated with DMSO (control) or dynasore (d) and respective quantification

of nuclear circularity (e), and nuclear area (f). Scale bar 10 μm . Three independent biological replicates; >234 cells/condition. Data are presented as box plots showing the 25th percentile (Q1), median, 75th percentile (Q3), and whiskers extending to the minimum and maximum values; statistical significance is indicated as *** $p < 0.001$. Statistical analyses were performed using two-tailed Mann-Whitney U-test (b: $p < 0.0001$, c: $p < 0.0001$, e: $p < 0.0001$, f: $p < 0.0001$). Dyns, Dynasore; WT, Wild-type.



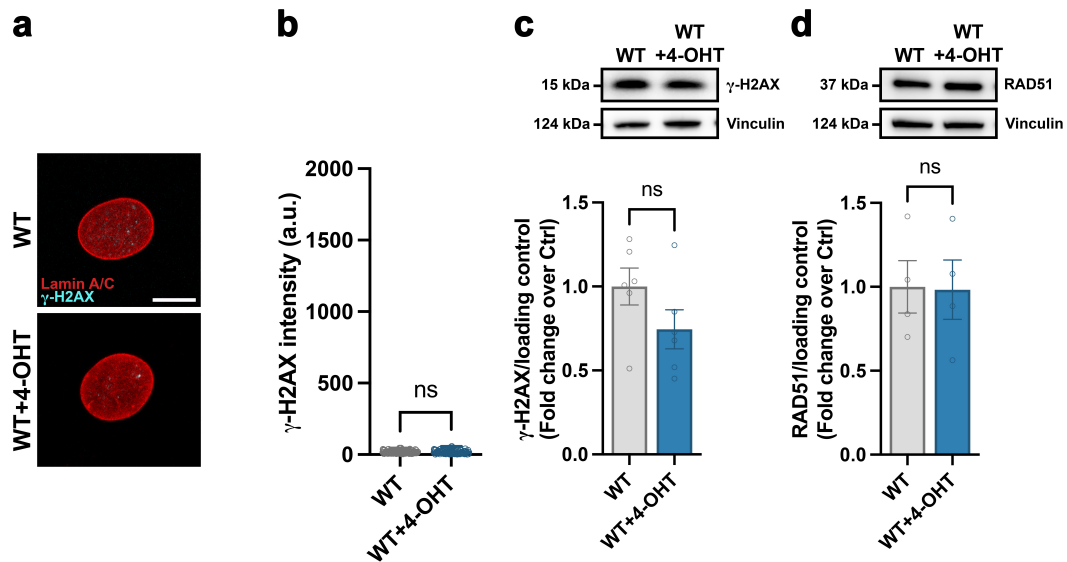
Supplementary Figure 5: Accumulation of dynamin-2 fluorescent signal in the nuclear proximity in live control and dynamin TKO cells.

(a) Western blots of lamin-A and lamin-C, and respective quantifications. No change in protein levels were observed upon 4-OHT treatment of WT fibroblasts with DMSO and 4-OHT for 12 days. Seven independent biological replicates. **(b)** Live-cell imaging of GFP-lamin A and dynamin2-K44A-mRFP mutant expressed in control cells for 24 hours by spinning-disk microscopy (red and green channels). Arrows show dynamin2-K44A signal in the nuclear proximity (as determined by GFP-lamin A signal) that persists for a long time, usually throughout the duration of imaging experiment (here shown at 1 min). Scale bar 5 μm . Exemplary data from three biological replicates. **(c)** Live-cell imaging of GFP-lamin A and dynamin2-WT-mRFP expressed in dynamin TKO cells for 22 hours by confocal microscopy. Note that NE buds were no longer enriched in rescued cells, and dynamin-2 enrichments were transient (1 image was taken every 4 min, a sequence of 8 images for a total of 28 min is shown). Arrows show examples of transient dynamin2 signal accumulation (overexpressed fluorescent dynamin-2 is mainly cytosolic) in the nuclear proximity (determined by GFP-lamin A signal). Scale bar 5 μm . Nuclear surface is shown in (a), in contrast to (b) in which optical cross-section through the cell is shown. Data are presented as bar charts with mean \pm SEM; statistical significance is indicated as ns, not significant. Statistical analyses were performed using two-tailed unpaired Student's t-test with Welch's correction (a: lamin A $p=0.6873$; lamin C $p=0.5709$). Ctrl, Control; TKO, Triple knockout.



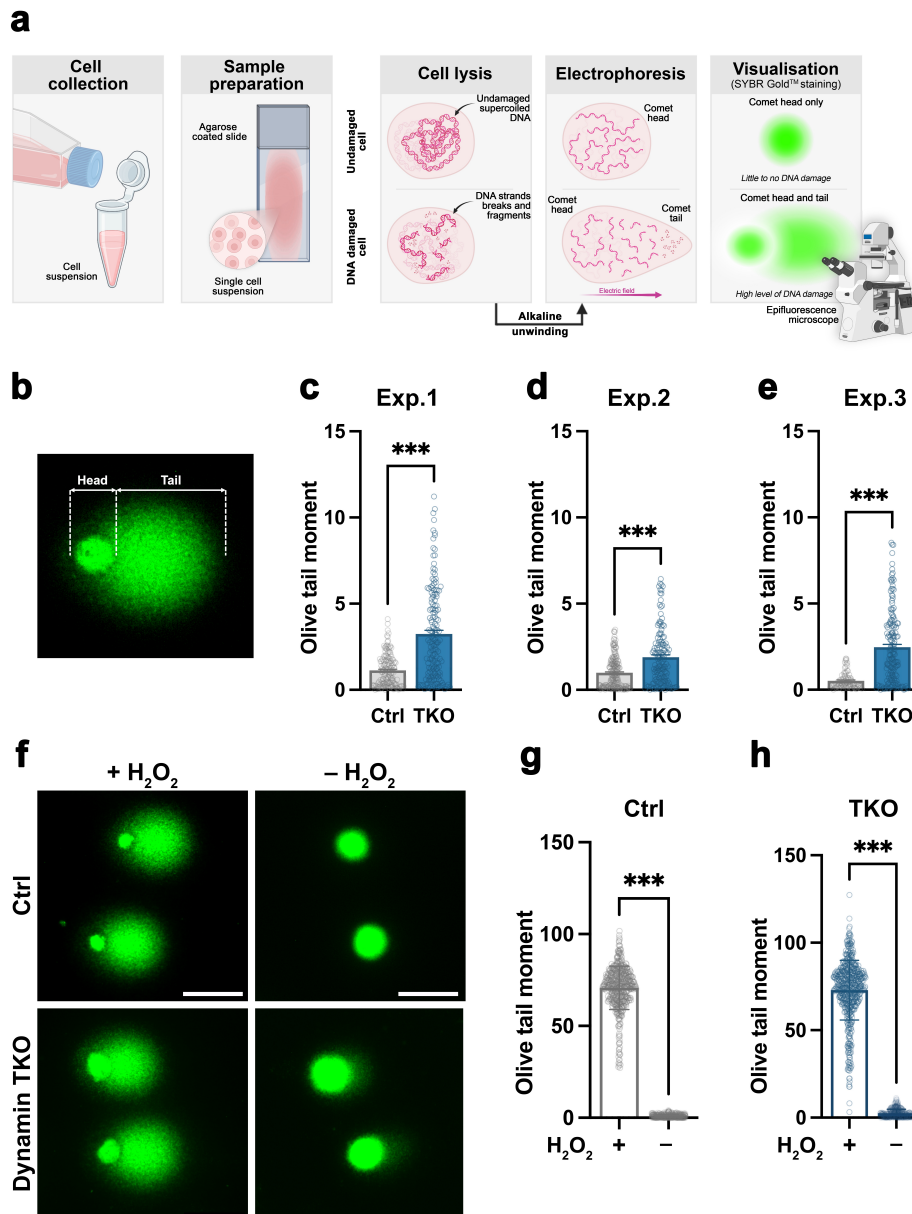
Supplementary Figure 6: Schematic workflow for ultrastructural analyses of nuclear envelope in dynamin TKO cells through FIB milling and cryo-ET.

(a) Schematic of a dynamin-TKO cells stably expressing GFP-lamin-A and co-stained with SPY555-DNA™ on an EM grids. A fluorescent green-red fluorescent z-stack was first acquired (middle panel) to help 3D targeting for accurate milling (bottom panel). **(b)** Schematic of the FIB milling process (top panel), starting by removing the bulk material (middle panel) until the obtaining a final ~200nm thick, electron transparent lamella (bottom panel). **(c)** Schematic of a post milled cell on grid. A final fluorescent stack was acquired on the lamella (middle and bottom panel) to validate the presence of the target before transfer into a TEM microscope. **(d)** Schematic of cryo-ET data acquisition on a lamella (top panel), with first the acquisition of a medium magnification montage (middle panel) used to guide the acquisition of several tilt-series that are reconstructed into 3D tomograms for further analysis (bottom panel).



Supplementary Figure 7: No increase in γ-H2AX signal upon treatment with 4-OHT

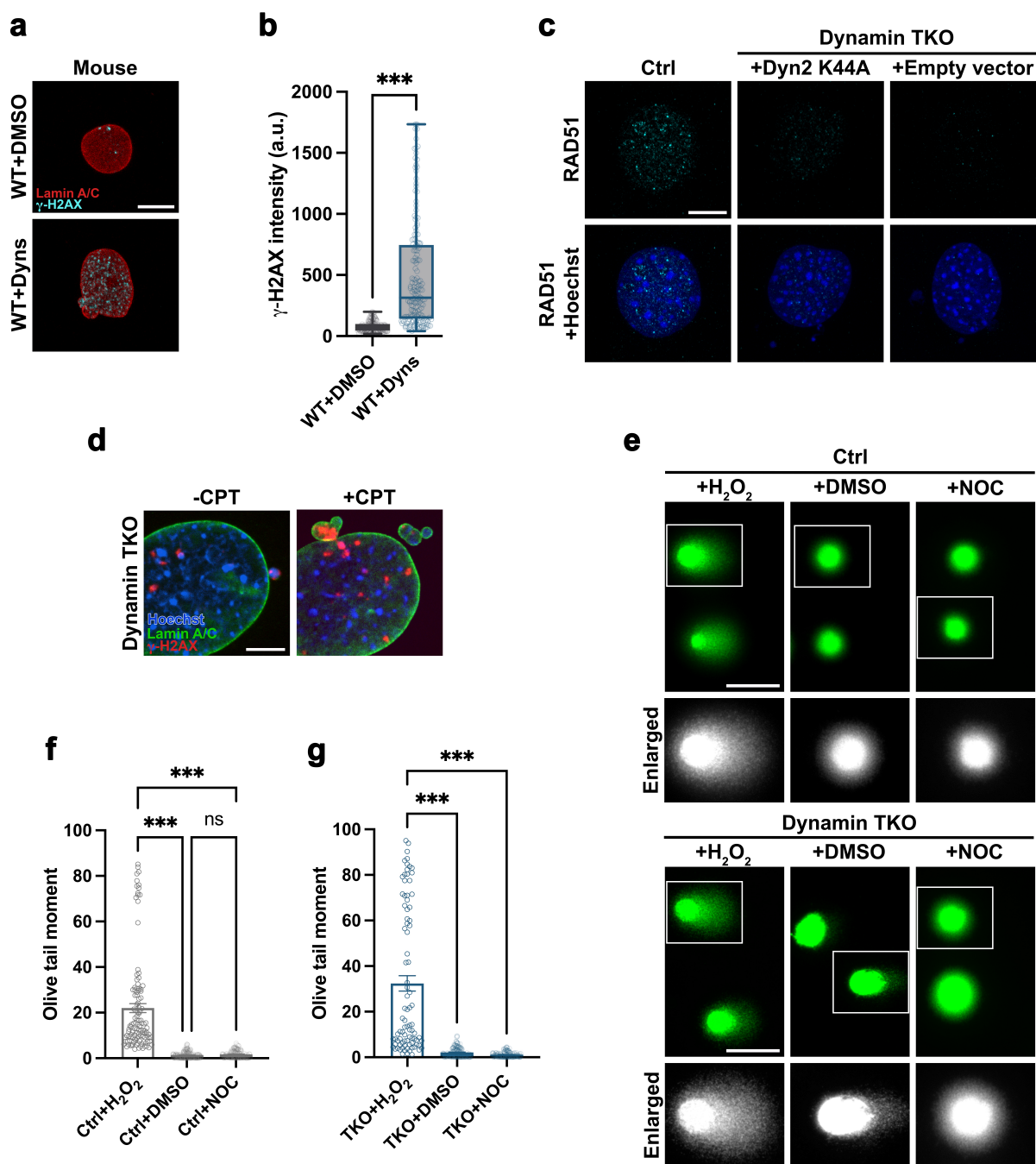
(a-b) Representative images of lamin A/C and γ-H2AX immunostained nuclei in WT mouse fibroblasts treated with DMSO (control) or 4-OHT as detailed in Methods, and respective quantification of γ-H2AX signal (b). Scale bar 10 μm. Three independent biological replicates; >102 cells/condition. **(c-d)** Western blot (top) and respective quantification (bottom) of γ-H2AX levels (c) and Rad51 (d) in control (DMSO-treated) and 4-hydroxytamoxifen (4-OHT)-treated WT cells after 12 days of treatments. Six (c) and four (d) independent biological replicates. Data are presented as bar charts with mean ± SEM; statistical significance is indicated as ns, not significant. Statistical analyses were performed using two-tailed Mann-Whitney U-test (b: $p=0.6834$) and two-tailed unpaired Student's t-test with Welch's correction (c: $p=0.1429$, d: $p=0.9432$). 4-OHT, 4-hydroxytamoxifen; Ctrl, Control; TKO, Triple knockout.



Supplementary Figure 8: Alkaline Comet assay reveals increased DNA damage in dynamin TKO cells.

(a) Schematic representation of the experimental approach used for alkaline Comet assay. Created in BioRender. Martial, T. (2026) <https://BioRender.com/dvrygaa>. **(b)** Definition of the parameters describing a comet. **(c-e)** Quantification of DNA damage (Olive tail moment = [tail mean-head mean] x % of DNA in the tail) after Comet assay under alkaline condition performed on control and dynamin TKO cells. Details from the three independent experiments as shown in Figure 3f; >90 cells/condition/experiment. **(f-h)** Representative images of control and dynamin TKO cells analysed by alkaline Comet assay in the presence or absence of H₂O₂ treatment (positive control) (f), and respective quantification of DNA damage (g,h). Scale bar 50 µm. Data from three independent biological replicates; >465 cells/condition. Data are presented as bar charts with mean ± SEM; statistical significance is indicated as ***p<0.001.

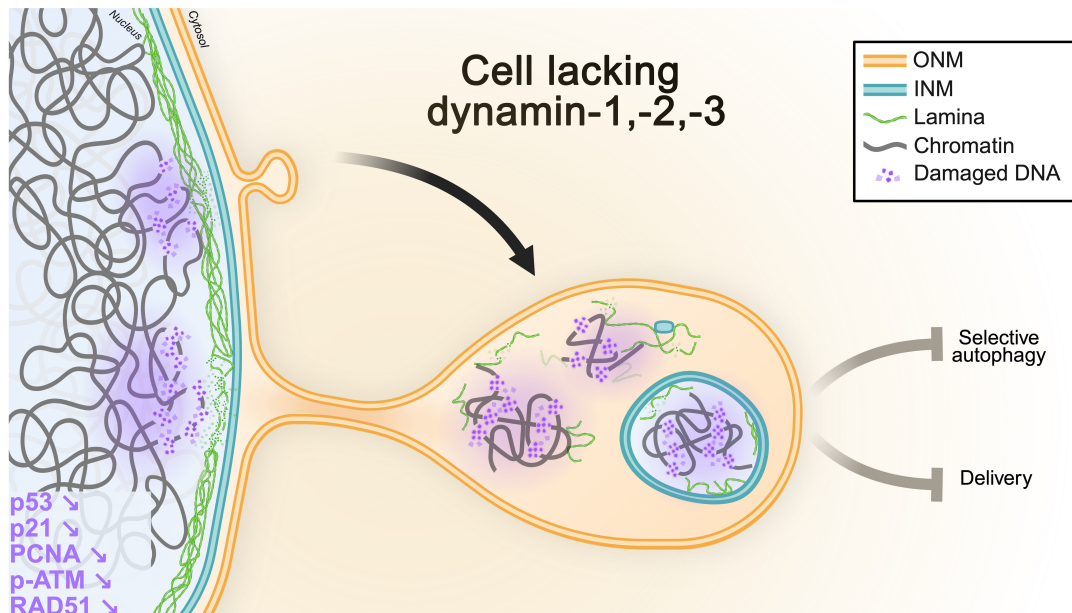
Statistical analyses were performed using two-tailed Mann-Whitney U-test (c: $p < 0.0001$, d: $p < 0.0001$, e: $p < 0.0001$, g: $p < 0.0001$, h: $p < 0.0001$). Ctrl, Control; TKO, Triple knockout.



Supplementary Figure 9: In addition to accumulation of nuclear dysmorphisms, pharmacological inhibition of dynamins and CPT treatment lead to accumulation of DNA damage in both mouse and human fibroblasts.

(a-b) Representative images of lamin A/C and γ -H2AX immunostained nuclei in wild-type mouse fibroblasts treated with DMSO (control) or dynasore (a), and respective quantification

of γ -H2AX signal (b). Scale bar 10 μ m. Examples from three independent biological replicates; >170 cells/condition. **(c)** Representative images of RAD51 (cyan) and Hoechst (blue) stained nuclei in control, dynamin-TKO, TKO expressing dynamin-2 and TKO expressing dynamin2-K44A for 24h. Scale bar 10 μ m. Quantification of these data is provided in Figure 6i. Examples from three independent biological replicates. **(d)** Representative images of lamin A/C, γ -H2AX and DAPI stained nuclei in dynamin TKO cells treated with DMSO (control) or camptothecin. Optical cross-sections through the cells are shown. Note that both number of NE buds and vesicles (dynamin strongly potentiates the membrane fission process, yet membrane fission can occur in its absence, as demonstrated by the presence of endosomal vesicles and synaptic vesicles in models without dynamins) is increased. Scale bar 5 μ m. Three independent biological replicates. **(e-g)** Representative images of control and dynamin TKO cells analysed by alkaline Comet assay in the upon H_2O_2 (positive experimental control), DMSO or nocodazole treatment (e), and respective quantification of DNA damage (f, g). Scale bar 50 μ m. Three independent biological replicates. >88 cells/condition. Data are presented as box plots showing the 25th percentile (Q1), median, 75th percentile (Q3), and whiskers extending to the minimum and maximum values. Statistical significance is indicated as ns, not significant; *** $p < 0.001$. Statistical analyses were performed using two-tailed Mann-Whitney U-test (b: $p < 0.0001$) and one-way ANOVA Kruskal-Wallis test followed by post-hoc Dunn's multiple comparisons test (f: $p < 0.0001$, $p = 0.2493$, $p < 0.0001$, g: $p < 0.0001$, $p < 0.0001$). CPT, Camptothecin; Dyns, Dynasore; NOC, Nocodazole; WT, Wild-type.



Supplementary Figure 10: Schematic depicting a proposed role for dynamins in the maintenance of nuclear envelope homeostasis and genome stability.

In the absence of all three dynamins, prominent dysmorphisms in the NE are observed, including the formation of nuclear buds with long narrow necks, reminiscent of the elongated clathrin-coated pit necks occurring at the plasma membrane in dynamin-deficient cells. These NE buds often accumulate damaged DNA and contain lamins A/C. This abnormal phenotype is rescued by the reintroduction of single wild-type dynamin protein or by nocodazole treatment, which both restored the NE dysmorphisms and reduced DNA damage, supporting the idea that dynamin, probably through its interaction with microtubules, plays a critical role in NE homeostasis and DNA damage clearance mechanisms. Notably, dynamin K44A mutant, which lacks GTPase activity, fails to rescue NE defects or prevent DNA damage accumulation in cells lacking dynamin, underlining the importance of dynamin GTPase activity in these processes. Created in BioRender. Raimundo, N. (2026) <https://BioRender.com/az0mexm>.

SUPPLEMENTARY TABLE 1

REAGENT or RESOURCE	SOURCE	IDENTIFIER
Antibodies		
Primary		
Mouse monoclonal anti-acetylated α -Tubulin	Sigma-Aldrich	T7451
Mouse monoclonal anti-dynamin (pan)	BD Transduction Laboratories	610245
Mouse monoclonal anti-HSP60	BD Transduction Laboratories	6111563
Mouse monoclonal anti-Lamin A/C	Santa Cruz Biotechnology	sc-376248
Mouse monoclonal anti-Lamin B1	Santa Cruz Biotechnology	sc-374015
Mouse monoclonal anti-PCNA	Santa Cruz Biotechnology	sc-56
Mouse monoclonal anti-SQSTM1	Abcam	ab56416
Mouse monoclonal anti-vinculin	Millipore	MAB3574
Rabbit monoclonal anti-alpha 1 Sodium Potassium ATPase	Abcam	Ab76020
Rabbit monoclonal anti-alpha-Tubulin	Cell Signaling Technology	2125
Rabbit monoclonal anti-cleaved capsase-3 (Asp175)	Cell Signaling Technology	9664
Rabbit monoclonal anti-p21	Abcam	ab188224
Rabbit monoclonal anti-RAD51	Cell Signaling Technology	8875
Rabbit polyclonal anti-ATM	Cell Signaling Technology	2873
Rabbit polyclonal anti-calnexin	Enzo	ADI-SPA-800-D
Rabbit polyclonal anti-GAPDH	Sigma-Aldrich	G9545
Rabbit polyclonal anti-LAMP1	Sigma-Aldric	L1418
Rabbit polyclonal anti-LC3B	Cell Signaling Technologies	2775
Rabbit polyclonal anti-p53	Proteintech	10442-1-AP
Rabbit polyclonal anti-phospho-ATM (Ser1981)	Cell Signalling Technologies	5883
Rabbit polyclonal anti-phospho-histone H2A.X (Ser139) (γ -H2AX)	Cell Signalling Technologies	2577

Secondary		
Goat anti-rabbit IgG, HRP-linked Antibody	Cell Signaling Technology	7074
Goat anti-mouse IgG (H+L) Highly Cross-Adsorbed Secondary Antibody, Alexa Fluor™ 568	Invitrogen, Thermo Fisher Scientific	A11031
Goat anti-mouse IgG (H+L) Highly Cross-Adsorbed Secondary Antibody, Alexa Fluor™ 488	Invitrogen Fisher Scientific, Thermo	A11029
Goat anti-rabbit IgG (H+L) Highly Cross-Adsorbed Secondary Antibody, Alexa Fluor™ 568	Invitrogen Fisher Scientific, Thermo	A11036
Goat anti-rabbit IgG (H+L) Highly Cross-Adsorbed Secondary Antibody, Alexa Fluor™ 488	Invitrogen Fisher Scientific, Thermo	A11034
Goat anti-rabbit IgG (H+L) Highly Cross-Adsorbed Secondary Antibody, Alexa Fluor™ 647	Invitrogen Fisher Scientific, Thermo	A21245
Horse anti-mouse IgG, HRP-linked Antibody	Cell Signaling Technology	7076
Chemicals and Reagents		
4-Hydroxytamoxifen, >=70% Z isomer	Sigma Aldrich	H6278
Acrylamide	BioRad	1610148
Agar	Labkem	AGAG-00P
Agarose LE	Biozym	840004
Agarose low melting (for Comet assay)	BioRad	1613111
Ammonium Persulfate (APS)	Sigma-Aldrich	A3678
Ampicillin	Carl Roth	K029.1
Bafilomycin A	Santa Cruz Biotechnology	sc-201550
Bicine	Acros Organics	327715000
Bovine serum albumin (BSA)	NZYtech/Sigma-Aldrich	MB47002/A9418
Bromophenol blue	Alfa Aesar	032639-06
Calcium chloride (CaCl ₂)	Alfa Aesar	L13191
Camptothecin (CPT)	Sigma-Aldrich	208925
CAPS	Fisher Bioreagents	BP321

Chemically Competent E. coli (DH5α)	New England Biolabs (NEB)	C2987
Deoxynucleotide dNTP Mix (10 mM each)	New England Biolabs (NEB)	N0447S
Dimethyl sulfoxide (DMSO)	Fisher/Sigma-Aldrich/ Thermo Fisher Scientific	BP231/D2650/ F-515
Dithiothreitol (DTT)	Fisher	BP172
DNA Ladder (1 kb)	Thermo Fisher Scientific	SM0311
DNA Loading Dye (6X)	Thermo Fisher Scientific	R0611
Dulbecco's Modified Eagles Medium (DMEM) high glucose (with 4500mg/L glucose, sodium bicarbonate, without L-glutamine)	Sigma-Aldrich	D6546
Dynasore hydrate	Sigma-Aldrich	D7693
ECL Prime Western Blotting Reagents Sample Kit	GE Healthcare	RPN2236
EDTA disodium salt	Sigma-Aldrich	E5134
Ethanol absolute	VWR/Sigma-Aldrich	20891.330/32221
Ethylene glycol bis(2-aminoethyl ether)tetraacetic acid (EGTA)	Fisher Chemicals	D/0755/46
Foetal Bovine Serum (FBS)	Gibco/Sigma-Aldrich	A5256801/F7524
Gelatine from cold water fish skin (for ICH)	Sigma-Aldrich	G7765
Gelatine from porcine	Sigma-Aldrich	G2500
Glycerol	Fisher Bioreagents/Sigma-Aldrich	BP229/G7757
Goat Serum	Gibco	16210-064
Halt™ Protease & Phosphatase Inhibitor Cocktail (100X)	ThermoFisher Scientific	1861284
Hydrochloric acid (HCl)	Sigma-Aldrich	30721
FluoroBrite™ DMEM	Gibco	
Kanamycin	Carl Roth	T832.2
<u>KLD Enzyme Mix</u>	New England Biolabs (NEB)	E0554S M0554AVIAL
Methanol	Enzymatic	VR0260
MG132	InVivoGen	TLRL-mg132
Magnesium Chloride (MgCl ₂)	Thermo Fisher Scientific	F-510Mg

Milkpowder, blotting grade	Oxoid	LP0033B
Mowiol® 4-88	Sigma-Aldrich	81381
Mutagenic Primers	Thermo Fisher Scientific	https://www.thermofisher.com/order/custom-standard-oligo/
Nocodazole	Sigma-Aldrich	487928-10MG
Nuclease-Free Water	VWR Chemicals	#436912C
NZYSoluble Protein Marker II	NZYSoltech	MB09002
PageRuler™ Plus Prestained Protein Ladder	Thermo Scientific™	26619
Paraformaldehyde (PFA)	ThermoFisher Scientific	416780010
Paraformaldehyde, 16%	Sigma-Aldrich	043368.9
Polyethylenimine (PEI)	Sigma-Aldrich	408727
Penicillin Streptomycin (Pen Strep)	Gibco	15140-122
Penicillin-streptomycin	Sigma-Aldrich	P0781
Phosphate buffered saline	Sigma-Aldrich	P4417
Phusion GC Buffer (5x)	Thermo Fisher Scientific	F-518
Phusion™ High-Fidelity DNA Polymerases (2 U/μL)	Thermo Fisher Scientific	F-530S
Poly-D-lysine	Gibco	A38904-01
Potassium chloride (KCl)	Sigma-Aldrich	P3911
Potassium dihydrogen phosphate (KH ₂ PO ₄)	Fisher Bioreagents	BP362
SiR-DNA	Spirochrome	SC007
SOC Medium	New England Biolabs (NEB)	B9020S
Sodium bicarbonate (NaHCO ₃)	Thermo Fisher	BP328
Sodium chloride (NaCl)	Sigma-Aldrich	31434
Sodium deoxycholate	Sigma-Aldrich	30970
Sodium dodecyl sulfate (SDS)	Sigma-Aldrich/ Invitrogen	L4509-500G/15525-017
Sodium hydroxide (NaOH)	Sigma-Aldrich	S5881
Sodium phosphate dibasic anhydrous (Na ₂ HPO ₄)	Fisher Bioreagents	10182863

SPY555-DNA	Spirochrome	SC201
SYBR [™] Gold	Sigma-Aldrich	S11494
Tetramethylethylenediamine (TEMED)	AppliChem	A1148,0025
Tris(hydroxymethyl)aminomethane (Tris)-Base	Fisher Bioreagents/ Sigma-Aldrich	BP152-5/T1503
Tris(hydroxymethyl)aminomethane (Tris)-HCl	Carl Roth/Sigma-Aldrich	9090.3/T3253
Triton X-100	Amresco/Carl Roth	694/3051.3
Trypan blue solution, 0.4%	Sigma-Aldrich	93595
Trypsin-EDTA (0.05%)	Gibco/Sigma-Aldrich	15400-054/T3924
Tryptone	VWR	84610.0500
Tween [™] 20	Thermo Fisher	BP337
Vectashield [®] antifade mounting medium	Vector Laboratories	H-1800
Verapamil	Spirochrome	From Spirochrome kits
WesternBright Sirius HRP substrate	GRISP	K-12043-D20
Yeast	Fisher Bioreagents	BP1422
Critical commercial assays		
Pierce [™] BCA Protein Assay Kit	ThermoFisher Scientific	Cat# 23225
DeadEnd [™] fluorometric TUNEL system	Promega	G3250
P4 Primary Cell 4D X Kit L	Lonza	Cat# V4XP-4024
Macherey-Nagel NucleoBond Xtra Midi (100)	Macherey-Nagel	Cat# 740410.100
Macherey-Nagel NucleoSpin Plasmid, Mini kit for plasmid DNA	Macherey-Nagel	Cat# 740588.50
Experimental models: Cell lines		
dynamin 1,2,3 conditional mouse fibroblasts	Park <i>et al.</i> , 2013	Gift/P. De Camilli
WT mouse fibroblasts	ATCC	SCRC-1008
Human dermal fibroblasts	ATCC	PCS-201-012
Lenti-X [™] 293T Cell Line	Takara Bio	632180

Recombinant DNA		
Dynamin 2-GFP		Gift/P. De Camilli
Dynamin 2-mRFP		Gift/P. De Camilli
Dynamin 2 R361S –mRFP		Generated in house
Dynamin 2 R399A –mRFP		Generated in house
GFP-Dynamin 2 K44A	Addgene	Plasmid #22301
Lamin A-mRFP	Addgene	Plasmid #124268
pEGFP-h53BP1	Addgene	Plasmid #110301
GFP-Lamin-A	Addgene	Plasmid #206027
pBABE-puro-GFP-wt-lamin A	Addgene	Plasmid #17662
pCDH_blast_MCS_Nard_GFP_LAMIN	Addgene	Plasmid #167340
pCMV delta R8.2	Addgene	Plasmid #12263
pEGFP-h53BP1 (siRNA resistant)	Addgene	Plasmid #110301
pHCMV-AmphoEnv	Addgene	Plasmid #15799
RFP Dynamin2 K44A	Addgene	Plasmid #128153
mEmerald-nesprin3	Addgene	Plasmid #54203
pmCherry-NLS	Addgene	Plasmid # 39319
pmRFP-LC3	Addgene	Plasmid #21075
Software and algorithms		
BioRender	BioRender (Toronto, Ontario, Canada)	https://www.biorender.com
cellSens (2021; version 3.2)	Olympus (Waltham, Massachusetts, USA)	https://www.olympus-us-lifescience.com/en/software/cellsens/
Fiji/ImageJ (2024; version 2.14.0/1.54f)	NIH (Bethesda, Maryland, USA)	https://imagej.net/Fiji/Downloads
GraphPad Prism 8, and GraphPad Prism 10 (2024; version 10.2.0)	GraphPad Software (Boston, Massachusetts, USA)	https://www.graphpad.com
Image Lab	BioRad (Hercules, California, USA)	https://www.biorad.com/en-uk/product/image-

		lab-softwareID=KRE6P5E8Z
Matlab (2023; version R2023b)	MathWorks (Natick, Massachusetts, USA)	https://www.mathworks.com/products/matlab.html
Microsoft 365 (2024; version 16.89.1)	Microsoft (Albuquerque, New Mexico, USA)	https://www.office.com
NEB Tm Calculator	New England Biolabs (NEB)	https://tmcalsculator.neb.com/#!/main
Photoshop (2024; version 25.5.1)	Adobe (San Jose, California, USA)	https://www.adobe.com/products/photoshop.html
SnapGene Viewer (2015; version 8.1.1.)	GSL Biotech LLC, USA	https://www.snapgene.com
Volocity (2008; version 4.3)	Quorum Technologies Inc. (Puslinch, Ontario, Canada),	https://www.volocity4d.com
ZEN black (2020)	Carl Zeiss AG (Jena, Saxe-Weimar-Eisenach, Germany)	https://www.zeiss.com/microscopy/en/products/software/zeiss-zen.html
ZEN blue (2020)	Carl Zeiss AG (Jena, Saxe-Weimar-Eisenach, Germany)	https://www.zeiss.com/microscopy/en/products/software/zeiss-zen.html

SUPPLEMENTARY METHODS

Plasmids

Dynamin 2-GFP and dynamin 2-mRFP were kind gifts from Prof Pietro De Camilli (Yale University, New Haven, USA). GFP-Dynamin 2 K44A (#22301), Lamin A-mRFP (#124268), pEGFP-h53BP1 (#110301), pCDH_blast_MCS_Nard_GFP_LAMIN (#167340), pCMV delta R8.2 (#12263), pHCMV-AmphoEnv (#15799), pEGFP-h53BP1 (siRNA resistant; #110301), RFP Dynamin2 K44A (#128153), mEmerald-Nesprin3 (#54203) were obtained from Addgene, pEGFP-N1 was obtained from Clontech (#6085-1). Dynamin 2 R361S–mRFP and Dynamin 2 R399A–mRFP were generated for this study as described in the paper.

Primers for site-directed mutagenesis

Mutagenic primers (R361S Forward: TGGTGGAGCCagcATCAATCGTA and Reverse: GACAACTCTAGTGTGTCTACTTG; R399A Forward: CCACGGAGTCgcgACTGGGCTCTTC and Reverse: ATGTTCTTAATAGCATAGCTGATC) were designed to introduce the desired point mutations in the *DNM2* coding region, and were verified for melting temperature using NEB Tm Calculator.

Additional information for Western blotting

Primary antibodies mouse anti-lamin A/C (Santa Cruz Biotechnology), mouse anti-lamin B1 (Santa Cruz Biotechnology), rabbit anti- γ -H2AX (Cell Signalling Technology), mouse anti-PCNA (Santa Cruz Biotechnology), rabbit anti-p53 (Proteintech), rabbit anti-p21 (Abcam), rabbit anti-phospho-ATM (Cell Signaling Technology), rabbit anti-ATM (Cell Signaling Technology), rabbit anti-RAD51 (Cell Signaling Technology), rabbit anti-LC3B (Cell Signaling Technology), mouse anti-SQSTM1 (Abcam), rabbit anti-LAMP1 (Sigma Aldrich), and mouse anti-dynamin (BD Transduction Laboratories) were used at a dilution of 1:1,000.

Additional information for live imaging by confocal microscopy

When indicated, 2 hours before live imaging sessions, SiR-DNA or SPY555-DNA (Spirochrome) was diluted to a final concentration of 200 nM in a growth medium (composition described in the Methods) supplemented with 10 μ M verapamil (Spirochrome), an efflux pump inhibitor. Live cell imaging by spinning-disk confocal microscopy was performed using the custom-made setup as detailed in the paper.

Live cell imaging of dynamin2-mRFP, GFP-lamin A and SiR-DNA (Spirochrome) was performed using an Olympus/Evident SpinSR SoRa spinning disc with Yokogawa CSU-W1 in spinning disc mode (50 μ m pinhole disc). Imaging was carried out using a 60x 1.3NA silicone oil objective. Detection was performed on a Hamamatsu ORCA Fusion BT camera set to 129 MHz read speed. mRFP (red) was captured using a B525/50 filter with excitation at 561 nm. GFP (green) and SiR-DNA (far-red) were captured using a quad band pass filter with excitation at 488 nm and 640 nm respectively. Exposure times and illumination values were as follows: Green - 60 ms - 6%; Red - 60 ms - 5%; Far-red - 60 ms - 4%. Seventeen Z sections were captured at 1 μ m spacing, every 4 min, across approximately 20 positions in Ibidi 8-well plates (Ibidi) for 32 hours. A humidified 5% CO₂ atmosphere and 37°C temperature control ensured sample viability.

Live cell imaging of GFP-lamin A (green) cells was performed using a Zeiss LSM 900 equipped with an Airyscan2 detector and with 405 nm, 488 nm, 561 nm and 647 nm excitation laser diodes. A 60x 1.2NA water lens was used with excitation at 488 nm (0.7%; 70 μ m pinhole; gain 650 V) to image the cells. Multiple xy positions were captured every 4 min, with 17 Z-sections

at 1 μm for 16 hours. An 84.5 μm field of view (FOV) was imaged at a resolution of 460x460 pixels using bi-directional scanning at a scan speed of 9.

TUNEL, propidiumiodine/AnnexinV-FITC, and trypan blue exclusion assays

The proportion of apoptotic cells was estimated using the DeadEnd™ Fluorometric TUNEL system kit (ProMega) according to manufacturer's instructions, with minor alterations. Briefly, cells were fixed in 4% (v/v) PFA in PBS at RT for 10 min, washed twice with PBS, and permeabilized in 0.2% (v/v) Triton X-100 for 5 min. After washing three times in PBS, samples were incubated in the equilibration buffer from the staining kit for 10 min. Coverslips were then incubated in the reaction mix, prepared according to the manufacturer's protocol, for 1 hour at 37°C in a dark humidified chamber. The reaction was terminated by washing coverslips twice in the 2x Saline Sodium Citrate (SSC) provided by the supplier for 7 min each, and coverslips mounted in Vectashield Antifade Mounting Medium with DAPI (Vector Laboratories). All wide-field epifluorescence images were captured using the Olympus SLIDEVIEW VS200 slide scanner (Olympus Life Science). Three images per coverslip were captured at a 40x magnification in randomly selected regions. Images were imported into ImageJ/Fiji software, and DAPI/Tunel overlay images were produced. TUNEL image analysis was automated using MATLAB version R2023b (The MathWorks) and a home-made script. Nuclei were segmented in the DAPI channel. TUNEL-positive nuclei were identified if the green channel intensity within a defined object (nucleus) exceeded a threshold (mean background intensity of the green channel in TUNEL negative cells plus 2 standard deviations).

For propidiumiodine (PI)/AnnexinV-FITC staining, control and dynamin-TKO cells were cultivated on coverslips overnight followed by PI/AnnexinV-FITC staining according to manufacturer's instructions (Thermo Fisher, V13242). Images containing 200+ cells were analyzed for fluorescence emission.

The cell viability is further assessed by trypan blue assay which stains dead cells blue, while live cells with intact membranes exclude the dye, remaining unstained. Same number of control and dynamin knock out cells (day 12 post-4-OHT treatment) were exposed to trypan blue dye (cell suspension/trypan blue 1:1) and counted using Countess 3 automatic cell counter (Invitrogen).

Cleaved caspase-3 assay

For cleaved caspase-3 immunofluorescence, cells were grown on poly-L-lysine-coated coverslips (Sigma-Aldrich). Cells were washed with pre-warmed PBS (pH 7.4) and fixed with 4% (w/v) PFA for 20 min at RT. Cells were washed with PBS and blocked with 3 % BSA/0.2% cold fish gelatine/1% goat serum/0.1% Triton X-100/PBS for 1 hour at RT to prevent non-specific binding. Cells were incubated with primary antibodies, diluted in the blocking solution,

overnight at 4 °C. The primary antibody used was rabbit anti-cleaved caspase-3 (1:400; Cell Signaling Technologies) and mouse anti-lamin A/C (1:200, Santa Cruz Biotechnologies). After incubation, cells were washed three times with PBS and incubated with the respective secondary antibody for 1 hour at RT. The secondary antibodies used were Alexa-Fluor 647-, and Alexa Fluor 594-conjugated goat anti-rabbit or anti-mouse IgG. Finally, coverslips were mounted on glass slides with Vectashield Antifade Mounting Medium with DAPI. Fixed cells were imaged on a Zeiss LSM 900 equipped with an Airyscan2 detector and with 405 nm, 488 nm, 561 nm and 647 nm excitation laser diodes. A 63x 1.4NA Oil objective was used for acquisition. DNA was labelled with DAPI (blue) with excitation at 405 nm (1.8%; 42 µm pinhole; gain 670 V), primary antibodies against cleaved caspase-3 were detected with a secondary Alexa Fluor 647 (far-red) with excitation at 640 nm (3.1%; 57 µm pinhole; gain 718 V) and primary antibodies against lamin A/C were detected with secondary Alexa Fluor 568 (red) with excitation at 561nm (2.7%; 50 µm pinhole; gain 680 V). Scanning was carried out at a resolution of 1437 x 1437 pixels with a 101 µm FOV (Nyquist sampling) at a scan speed of 7, with 4x averaging, mono-directional, with detection on GaAsP-PMTs.

For image analysis, using ImageJ/Fiji small uniform squares (regions of interests) were defined for each cell, outside of the nucleus. Intensity and background were measured, before the background intensity was subtracted (background was indexed per image). Per biological replicate, 10 images were analysed per condition.